Nanoscale

RSC Publishing

PAPER

View Article Online
View Journal | View Issue

Cite this: *Nanoscale*, 2013, **5**, 9357

Assembly and organization of poly(3-hexylthiophene) brushes and their potential use as novel anode buffer layers for organic photovoltaics†

José Alonzo,[a] W. Michael Kochemba,[b] Deanna L. Pickel,[c] Muruganathan Ramanathan,[c] Zhenzhong Sun,[d] Dawen Li,[d] Jihua Chen,[c] Bobby G. Sumpter,[ce] William T. Heller[a] and S. Michael Kilbey II*[b]

Received 1st May 2013
Accepted 27th July 2013

DOI: 10.1039/c3nr02226a

www.rsc.org/nanoscale

Buffer layers that control electrochemical reactions and physical interactions at electrode/film interfaces are key components of an organic photovoltaic cell. Here the structure and properties of layers of semi-rigid poly(3-hexylthiophene) (P3HT) chains tethered at a surface are investigated, and these functional systems are applied in an organic photovoltaic device. Areal density of P3HT chains is readily tuned through the choice of polymer molecular weight and annealing conditions, and insights from optical absorption spectroscopy and semiempirical quantum calculation methods suggest that tethering causes intrachain defects that affect co-facial π-stacking of brush chains. Because of their ability to modify oxide surfaces, P3HT brushes are utilized as an anode buffer layer in a P3HT-PCBM (phenyl-C_{61}-butyric acid methyl ester) bulk heterojunction device. Current–voltage characterization shows a significant enhancement in short circuit current, suggesting the potential of these novel nanostructured buffer layers to replace the PEDOT:PSS buffer layer typically applied in traditional P3HT–PCBM solar cells.

Introduction

Interest in organic photovoltaic (OPV) materials and devices is driven by the need to meet the growing global energy demand using sustainable energy sources as well as by the compelling potential for producing low-cost, flexible solar energy devices using solution-based, high-throughput methods such as roll-to-roll processing. Presently, the most efficient and promising OPV devices have been made by blending donor and acceptor materials to create bulk heterojunction (BHJ) active layers, which are marked by large interfacial areas formed due to separation of donor and acceptor materials into domains of nanoscale dimension.[1–4] In addition to having domain sizes commensurate with exciton diffusion lengths and providing the driving force for dissociation of tightly-bound electron–hole pairs (excitons), the BHJ active layer must provide connected pathways for electrons and holes to reach the cathode and anode, respectively. As a result, it is generally accepted that improving and optimizing the power conversion efficiency (PCE) of devices requires control of the BHJ nanoscale morphology. This realization has motivated numerous studies of the role of solvent type, donor–acceptor blend ratio, annealing conditions, and additives on the morphology of the active layer and the resultant PCE.[1–8]

The nature of the electrode/active layer interfaces also plays a significant role in the performance of an OPV device, as these interfaces control the collection and extraction of charge carriers. Buffer layers that break device symmetry and enhance hole collection at the anode or electron collection at the cathode by adjusting barrier heights and that promote good interfacial contact have proven to be essential ingredients for maximizing device performance.[9–11] In addition, and as is the general case for polymer thin films, surface-modifying layers alter interactions across the surface/thin film interface, changing wetting characteristics and affecting the segregation and organization of material at the interface and the final film structure.[12,13] Thus buffer layers must satisfy complex and perhaps competing tensions to achieve a proper balance between physical interactions and electrochemical reactions at cell/electrode interfaces in order to optimize OPV device performance. The complexity of this dual role is exemplified in the work of Germack *et al.*,[5,6] who showed that the surface energy dramatically impacts the interfacial composition of a BHJ thin film made from a blend of poly(3-hexylthiophene) and phenyl-C_{61}-butyric acid methyl ester

[a]*Biology and Soft Matter Division, Oak Ridge National Laboratory, Oak Ridge, TN 37831, USA*

[b]*Departments of Chemistry and of Chemical and Biomolecular Engineering, University of Tennessee – Knoxville, Knoxville, TN 37996, USA. E-mail: mkilbey@utk.edu*

[c]*Center for Nanophase Materials Sciences, Oak Ridge National Laboratory, Oak Ridge, TN 37831, USA*

[d]*Department of Electrical and Computer Engineering and Center for Materials for Information Technology, University of Alabama, Tuscaloosa, AL 35487, USA*

[e]*Computer Science and Mathematics Division, Oak Ridge National Laboratory, Oak Ridge, TN 37831, USA*

† Electronic supplementary information (ESI) available: TGA and DSC analysis of the P3HT-3K and P3HT-4K materials. See DOI: 10.1039/c3nr02226a

(P3HT and PCBM, respectively). Using near-edge X-ray absorption fine structure spectroscopy and a model substrate to mimic the surface energy established when an anode is coated with a layer of poly(3,4-ethylene dioxythiophene):poly(styrene sulfonate) (PEDOT:PSS), they showed that the anode/BHJ film interface was substantially enriched in PCBM (18 vol% P3HT) while the free surface, where the cathode would be deposited, was dominated by P3HT (74 vol% P3HT).[5] Because of the dominance of donor material (P3HT) at the cathode and PCBM acceptor at the anode, this type of vertical phase segregation is likely to negatively impact OPV device performance. In addition, this "inverted" morphological structure has been observed in neutron reflectometry experiments, which are sensitive to the laterally-averaged composition profile of the active layer normal to the substrate.[7,8] As a result, and also because of the inherent acidity and hygroscopic nature of PEDOT:PSS and the fact that it is not charge selective,[14,15] researchers have sought alternatives to the PEDOT:PSS dispersions that are typically applied to the anode.[9,10,14–17]

Because they straddle interfaces, polymer brushes are one way to alter structure and properties at substrate interfaces. By modifying the polymer chains to include reactive end groups, it is possible to decorate surfaces with polymer chains, thereby imparting new or adjusting specific physical and chemical properties of the interface by manipulating the spatial extent of the tethered chains, their grafting density, or chemical constituents. While polymer brushes based on flexible chains have been studied for over 20 years and applied in a variety of technologies,[18–25] because of difficulties associated with adapting the polymerization methods for surface-initiated growth or because of the limited solubility of π-conjugated polymers, there are only a few reports of well-defined semi-rigid polymer brushes based on π-conjugated polymers.[26–30]

Here we describe the formation and characterization of well-defined P3HT brushes created using a "grafting to" approach. We show that the methodology is applicable to silicon, quartz and ITO substrates, and allows the grafting density of chains to be easily tuned. In addition to creating P3HT brushes marked by high grafting density, a particular hallmark of this work is that because pre-made P3HT chains are grafted to the substrates rather than grown from surface-tethered initiators, rigorous macromolecular characterization can be brought to-bear for a more thorough understanding of the structure of the brush layers, which cannot be done in the case of chains grown from surface-tethered initiators. These features provide an avenue for understanding synthesis–structure–property relationships of devices based on P3HTs brushes. Finally, the performance of a solar cell that uses a P3HT brush as an anode buffer layer is compared to an analogous device made with the commonly used PEDOT:PSS buffer layer.

Experimental

Synthesis and brush formation

P3HT polymer brushes were formed from end-functionalized P3HTs bearing a trichlorosilane group. Regio-regular P3HTs were made by Grignard metathesis (GRIM) polymerization of the regiospecific monomer prepared from 2,5-dibromo-3-hexylthiophene,[31–34] followed by *in situ* quenching using a Grignard reagent to install a terminal alkene at the chain end.[32] Hydrosilation of the terminal alkene using tricholosilane (Aldrich, 99%) was carried out as described by Sullivan and coworkers.[35] Two different molecular weight P3HTs were used as starting materials, denoted throughout this article as P3HT-3K and P3HT-4K. The GRIM polymerization of P3HT-3K was quenched using allylmagnesium bromide while P3HT-4K was quenched using vinylmagnesium bromide. The chemical structures of the two polymers are shown in Fig. 1. Molecular weights were determined by Matrix Assisted Laser Desorption Ionization Time-of-Flight mass spectrometry (MALDI-TOF MS) using *trans*-2-[3-(4-*t*-butyl-phenyl)-2-methyl-2-propenylidene]-malonitrile (DCTB) as the matrix and polydispersity indices (PDI) were determined using size exclusion chromatography (SEC) in tetrahydrofuran relative to polystyrene standards.

Because of the various characterization methods applied, silicon wafers (Silicon Quest International, [1,1,1]), quartz slides, and indium tin-oxide coated glass slides (Delta Technologies, sheet resistance ~35 Ω) were used as substrates. Silicon wafers and quartz substrates were cleaned by immersion in piranha acid solution (3 : 1 v/v H_2SO_4 : H_2O_2) at 90 °C for 15 minutes and then rinsed with copious amounts of deionized (DI) water before being blown dry with a stream of nitrogen. (*Caution!* Piranha acid is a strong oxidizer and a strong acid that reacts violently with organic compounds.) ITO-coated glass substrates would be rapidly etched by the piranha acid solution; therefore, these substrates were washed using soap and water, sonicated twice for 15 minutes in DI water followed by sonication for 15 minutes in acetone (Aldrich, >99.5%) and then for 15 minutes in isopropyl alcohol (Aldrich, >99.5%). After drying with a stream of nitrogen, the ITO-coated glass substrates were subjected to 20 minutes of UV-ozone treatment.

Trichlorosilane-capped P3HT chains were attached to the various substrates to create P3HT brushes, which are shown schematically in Fig. 1. Chloroform solutions containing the end-functionalized P3HT (nominally 0.5 wt%) were used to deposit a thin film of the polymer on the substrate by

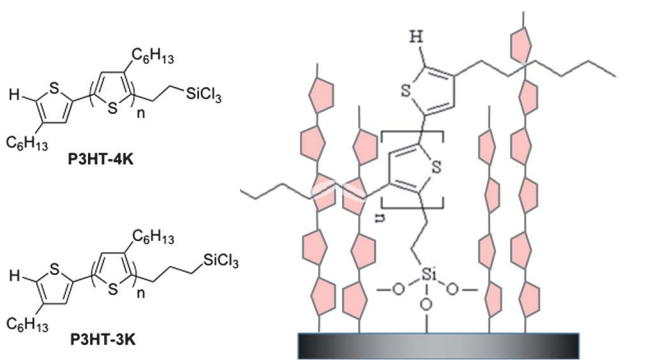

Fig. 1 (left) Chemical structures of the P3HT-3K and P3HT-4K tricholorsilane end-functionalized P3HTs used for brush formation. (right) Schematic of a P3HT brush made by end-grafting trichlorosilane-terminated P3HTs to silicon (or quartz or ITO) surfaces.

spin-coating at 1000 rpm for 30 seconds. Immediately after the deposition process, the samples were transferred to a vacuum oven and annealed for 24 h. The P3HT-3K brushes were annealed at either 120 °C, 150 °C or 190 °C, while the P3HT-4K brushes were annealed at either 120 °C, 150 °C, 190 °C or 250 °C. The samples were allowed to cool to room temperature in the vacuum oven before being immersed in chloroform and sonicated for 1 h to remove any non-grafted chains.

Materials and device characterizations

Ultraviolet-visible spectroscopy (UV-vis). A Varian Cary 5000 spectrophotometer (Agilent Technologies, Santa Clara, CA) was used to measure the optical absorbance of films deposited on quartz and ITO-coated glass substrates. Measurements were performed over a wavelength range from 200 nm to 800 nm, and background spectra were collected for the clean, blank substrates to correct the absorbance.

Ellipsometry. A J. A. Woollam M-2000U variable angle spectroscopic ellipsometer was used to measure the thickness of the brushes formed on silicon surfaces. Estimates of the film thickness were determined by fitting the data between 750 nm and 900 nm using a model based on three slabs of uniform optical density.[6] The slabs in the model consisted of bulk silicon (1 mm thick), silicon dioxide (1.5 nm) and the P3HT brush, which was described by a Cauchy model, with the layer thickness and model constants treated as fitting parameters. The thicknesses reported are the average of at least 3 different measurements from each sample.

Atomic Force Microscopy (AFM). The surface topography of the films and film-free substrates were imaged with a Dimension 3100 scanning probe microscope (Veeco Instruments, Plainview, NY, USA). Height and phase images over a 2 μm × 2 μm area were simultaneously collected in tapping model using a SiN tip. The root mean-square roughness values obtained from the images collected were determined using the analysis software supplied with the instrument.

OPV device formation and characterization. Photovoltaic devices were fabricated by dissolving a blend of P3HT and PCBM (1 : 0.7 by mass) in 1,2-dichlorobenzene (DCB) at a concentration of 20 mg ml^{-1}. A brush-modified ITO glass substrate was prepared as described above and used immediately after removal of any non-bonded P3HT. For the control cell, the ITO glass substrates were cleaned as described previously, then placed on a hot plate at 140 °C for 20 minutes to simulate the heat treatment experienced when brushes are grafted onto ITO surfaces. After cooling, filtered PEDOT:PSS (H. C. Stark) was spin-coated onto the ITO-coated glass substrate at 5000 rpm for 40 s and then dried at 140 °C for 10 min on a hotplate. The P3HT/PCBM solution in DCB was spin-coated onto the brush-modified or PEDOT:PSS-modified ITO substrates at 900 rpm for 40 s inside an argon filled glove box. These substrates were then annealed at 140 °C for 20 min in a vacuum oven. After annealing, the top metal cathode (15 nm Ca and 85 nm Al) was thermally evaporated under vacuum (~3×10^{-7} Torr) using a shadow mask. Current–voltage (*I–V*) characterization of the polymer photovoltaic cells was performed using a computer-controlled measurement unit from Newport Corporation (Irvine, CA) under an illumination of AM1.5 G, 100 mW cm^{-2}. All device measurements were performed inside an argon filled glove box.

Results and discussion

The molecular properties of the P3HT-3K and P3HT-4K polymers prepared for the interfacial layer formation are summarized in Table 1. While both materials have low polydispersities, the molecular weights determined by MALDI and by SEC are different because P3HT is a semi-rigid polymer whose molecular weight is overestimated by SEC and also because the absolute molecular weight determined by MALDI-TOF MS is sensitive to the extraction process.[31,36] The *in situ* end-capping of the GRIM polymerization using allylmagnesium bromide or vinylmagnesium bromide is known to produce monofunctional P3HTs in near-quantitative yields.[32] Regioregularity of the resultant polythiophenes, as estimated by ^{1}H NMR spectroscopy using a combination of the aryl proton and methylene protons of the hexyl side chains,[37,38] is high (>95%) and comparable. Thermogravimetric measurements (Fig. S1 in the ESI† file) indicate that the two P3HTs decompose above 400 °C and should, therefore, not degrade significantly during annealing. DSC heat flow traces (Fig. S2 in the ESI† file) recorded on the allyl- and vinyl-terminated analogs confirm that melting transition temperatures, T_m, are similar: $T_m = 216$ °C for P3HT-3K and $T_m = 208$ °C for P3HT-4K.

The thicknesses of the layers determined by ellipsometry as a function of annealing temperature are presented in Fig. 2 along with grafting densities that are calculated based on the molecular weights determined using MALDI-TOF MS. The measured thickness, t, is related to the areal grafting density, σ, by $\sigma = t\rho N_{Av}/M_n$, where ρ is the bulk density of the polymer (assumed to be 1.1 g cm^{-3}), N_{Av} is Avogadro's number, and M_n is the number average molecular weight. When annealed at 120 °C or 150 °C for 20 minutes, spin coated films made using P3HT-3K and P3HT-4K produce interfacial layers having similar thicknesses. The P3HT-3K consistently produces much thicker layers when annealed at 190 °C, but the increase in layer thickness and grafting density is more gradual for the P3HT-4K and there is no sharp increase even when the films are annealed at 250 °C. The different behaviors observed most likely originate in the molecular characteristics of the P3HTs. The larger chain length of the P3HT-4K, including a population of longer chains resulting from the higher polydispersity, may decrease the average accessibility of the reactive trichlorosilane groups to the substrate, resulting in lower grafting densities. Also, the extra methylene unit present in the allyl-terminated P3HT-3K (not

Table 1 Molecular characteristics of end-functionalized P3HTs

Polymer	M_n[a] (g mol^{-1})	M_n[b] (g mol^{-1})	PDI[b]	Regioregularity[c]
P3HT-3K	3400	9000	1.16	>95%
P3HT-4K	4300	9600	1.25	>95%

[a] Determined by MALDI-TOF MS. [b] Determined by SEC in THF *versus* polystyrene standards. [c] Estimated by ^{1}H NMR.

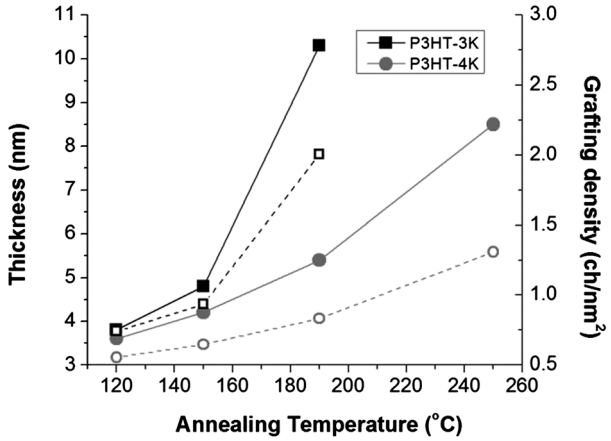

Fig. 2 Thickness (filled markers) and grafting densities (hollow markers) for end-tethered layers formed from the P3HT-3K (squares) and P3HT-4K (circles) polymers as a function of annealing temperature.

present in the vinyl-terminated P3HT-4K) may provide additional conformational freedom that relieves steric hindrance resulting from the hexyl side chain being proximal to the trichlorosilane end group, thereby enabling more trichlorosilane-capped chains to reach and react with hydroxyl groups on the surface.

These results demonstrate that controlling the annealing temperature provides a facile way to manipulate the layer thickness and grafting density. It is tempting to refer to the end-tethered layers as P3HT brushes because of the single-point attachment as well as the concomitant increase in thickness with chain crowding; however, P3HT is generally not considered to be a flexible polymer. For flexible polymers the brush regime is often benchmarked by the relation $d/2R_g < 1$, which compares (one-half of) the distance between chain tethering points, d, to the radius of gyration of the free chain, R_g.[22,25] While d can be calculated from the grafting density,[25] reports of R_g of P3HTs are rare. This is ostensibly due to ambiguity resulting from disagreement between molecular weights obtained by MALDI-TOF MS and by SEC, as well as the optical absorbance and low solubility of conjugated polymers that complicate light scattering measurements. To make a reasonable approximation, we use the Kratky–Porod worm-like chain model based on the weight-average molecular weight as determined by MALDI-TOF MS. This model is parameterized using a persistence length of 2.4 nm, which was determined by Heffner and Pearson[39] for regio-irregular P3HTs in THF and found to be relatively insensitive to the moment of the molecular weight distribution, and a monomer size of 0.36 nm, which was determined by *ab initio* calculation.[40] This treatment results in $d/2R_g$ values that range from 0.18 for the P3HT-3K at the highest σ to 0.31 for the P3HT-4K at the lowest σ.[41] As these two cases bracket all of the surface-tethered P3HT layers produced, they confirm that the P3HT chains are laterally crowded in a manner consistent with brush-like structures, as represented schematically by the drawing shown in Fig. 1.

Some useful insight can be gained by examining the thickness of the tethered P3HT layer, t, relative to the size of the coil, $t/2R_g$. Using R_g values based upon molecular weight determined by MALDI-TOF MS results in a range of $0.8 < t/2R_g < 2.3$ for P3HT-3K and $0.7 < t/2R_g < 1.7$ for P3HT-4K.[41] If the layers are considered to be comprised of a single layer of end-tethered chains, then these values suggest that at the highest grafting densities achieved, the chains of the brush are stretched about twice their extent as a coil. This degree-of-stretching is not unreasonable, particularly in light of the known caveats associated with determining molecular weight of P3HTs[31,36] as well as results from Luzinov and co-workers, who showed that end-grafted, polystyrene brushes of moderate molecular weight displayed $t/2R_g = 1.5$–3.[42] As they point out, grafting end-functional chains from the melt state, rather than from solution, benefits from the screening of excluded volume interactions and also allows many chains to be in close proximity to the grafting surface, resulting in higher grafting densities and thicknesses.[42]

Fig. 3 shows the UV-vis spectra collected for the P3HT-3K brushes formed on quartz substrates after annealing and subsequent removal of the unattached polymer chains. The spectra have a single peak centered near 510 nm with a slight shoulder at ~600 nm that results from interchain processes brought on by aggregation.[43,43] Analogous to the behavior of semi-rigid poly(cyclohexadiene) brushes,[30] the peak height scales linearly with the ellipsometric thickness of the brushes and, therefore, with the amount of tethered P3HT chains. Spectra collected after spin coating and annealing but prior to removal of the unattached chains are also shown in Fig. 3. These spectra are consistent with the absorption spectrum expected for P3HT, and they also indicate that spin coating deposits a comparable amount of trichlorosilane-terminated P3HT polymer. The fact that the detailed shape of the UV-vis spectra of the P3HT brushes does not contain the well-defined features observed in the spectra of thicker as-coated films or in the annealed films (prior to removal of any free chains) may be simply due to the short path length (thinness) of the brushes and low signal, or it may reflect a difference in how the P3HT

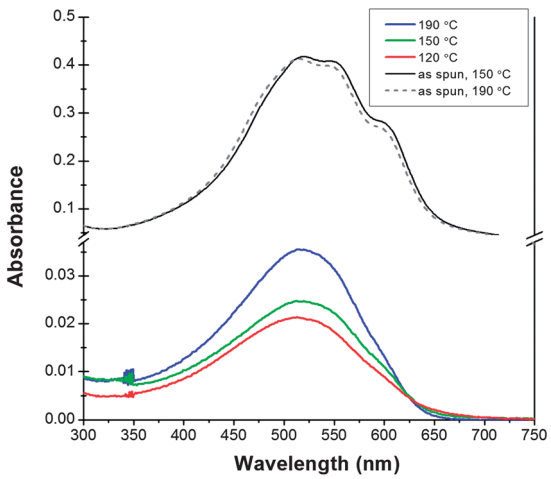

Fig. 3 UV-vis spectra of P3HT-3K brushes formed at 120 °C (red) 150 °C (green) and 190 °C (blue) along with the spectra of the as-spun P3HT-3K films after annealing at 150 °C (grey dotted) and at 190 °C (black).

chains aggregate when confined by end-tethering. In the context of Spano's treatment of the photophysics of aggregates of P3HT chains, an increase in orientation defects – such as torsional defects or kinks that prevent chain organization by co-facial π-stacking – brought about by tethering of the chain-like molecules would, in general, broaden spectral features because of an increase in energetic site disorder.[43] A minor but worthwhile comparison to note is that the FTIR spectra collected for P3HT powder and the P3HT brushes on silicon substrates (data not shown) are mutually consistent, with each showing the expected vibrational modes for the hexyl side chains and aromatic ring stretching modes.[45]

A series of calculations were performed to confirm that the shape of the UV-vis absorption spectra results from defects. Given a reasonable approximation of the electronic ground state, there are several methods that can be used to probe the electronic excited states.[46] A simple but effective approach is to use semiempirical quantum methods, in particular those developed by Zerner *et al.*,[47,48] based on parameterizing the INDO method on the basis of fairly extensive spectroscopic data (sometimes referred to as INDO/s or ZINDO/s). This approach when combined with configuration interaction singles (CIS), has been very successful for describing a variety of vertical electronic transitions, including π–π* transitions.[49]

CIS-ZINDO/s calculations of 3-hexylthiophene oligomers (12-mers) were used to estimate the transition energies and oscillator strengths. As seen in Fig. 4, an isolated P3HT 12-mer without conformational defects shows a single sharp peak for the singlet transition, and a small shoulder arises when three 12-mers are aggregated in a single co-facial π-stack. This effect of π-stacking is a well-accepted behavior.[43,44] The sharp singlet transition observed in both of these spectra is split when a second π-stack, also containing three 12-mers (with no conformational defects), is added to the system. Finally, to address the impact of intrachain defects, one conformational defect was added to each chain (P3HT 12-mer) in a system comprising 2 lateral π-stacks (of three 12-mers each). The well-resolved splitting of the main singlet transition disappears and the shoulder due π-stacking is significantly attenuated. These results support the interpretation that the detailed shape of the UV-vis spectra of the P3HT brushes could originate from intrachain defects that interrupt interchain contributions to the absorption spectra.

AFM was used to characterize the surface topography of the brush-modified substrates after removal of the unattached polymer chains. The images, shown in Fig. 5, indicate uniform coverage of the substrates, which has been somewhat difficult to attain when orthogonal "click" reactions were used to attach azido-terminated P3HTs to alkyne groups decorating a solid substrate[26] or during early stages of growth from surface-tethered initiators.[27] In the case of the quartz and ITO substrates, attachment of the P3HT chains decreases the root mean square (RMS) roughness values (from 2.6 nm to 1.7 nm for P3HT-grafted onto quartz and from 3.0 nm to 2.1 nm for P3HT grafted onto ITO), indicating that the brush fills features on the substrate.

A P3HT brush-modified ITO substrate was used to fabricate an OPV device, creating an ITO/P3HT brush/P3HT-PCBM/Ca/Al architecture. The performance of this device was compared to a traditional P3HT-PCBM bulk heterojunction device having an

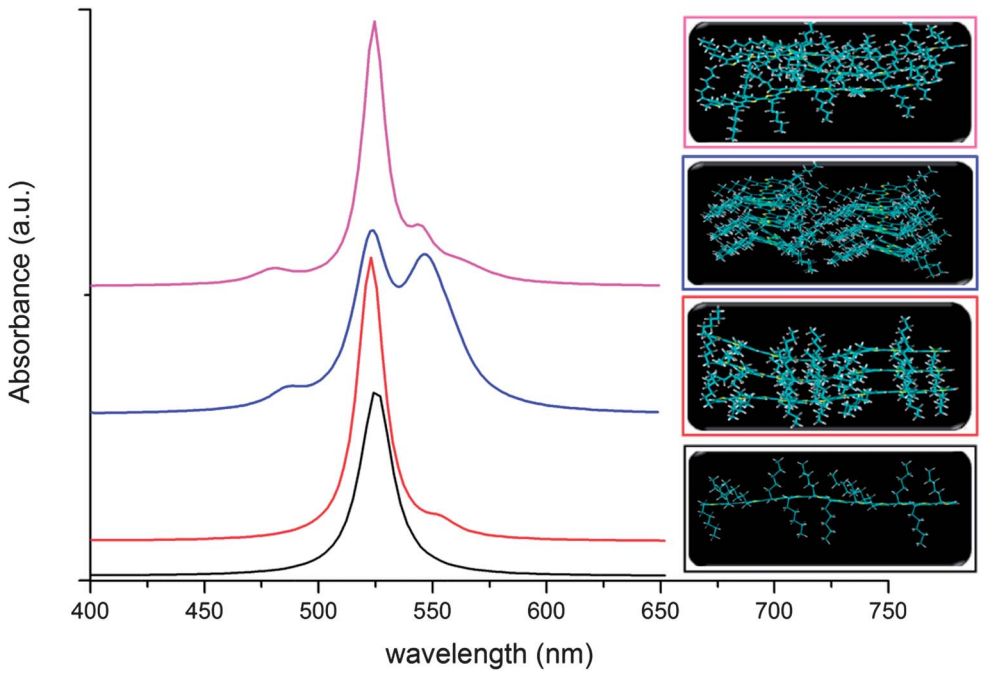

Fig. 4 Calculations of optical absorption spectra of P3HT oligomers using the semiempirical quantum method CIS-ZINDO/s. The most intense oscillator strengths, which correspond to the singlet transition, were shifted to coincide with the corresponding maximum measured by experiment. Each of the inset optimized structures is encircled with a line having a color that corresponds to the calculated spectrum: black: single 12-mer P3HT chain; red: one co-facial π stack of three 12-mers; blue: two lateral π stacks each containing three co-facially stacked 12-mers; and pink: one stack of three 12-mers, each with a single conformational defect.

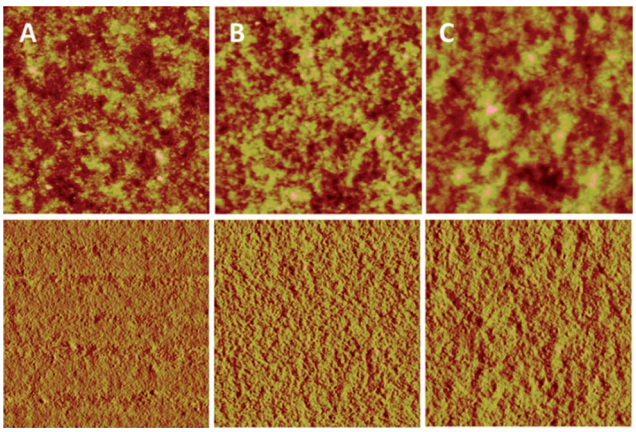

Fig. 5 AFM height (top) and phase (bottom) images acquired for the P3HT brushes formed on silicon (A), quartz (B), and ITO-coated glass (C) substrates. All images are 2 μm × 2 μm.

ITO/PEDOT:PSS/P3HT-PCBM/Ca/Al architecture. In the former, a P3HT brush was formed using P3HT-4K annealed at 150 °C in place of the PEDOT:PSS buffer layer commonly used to break the symmetry of BHJ devices and selectively transport holes to the anode. Device performance *I–V* curves were measured under AM1.5G illumination as shown in Fig. 6, and the device performance characteristics are presented in Table 2.

The performance of the photovoltaic device created with the P3HT brush demonstrates the potential of these interfacial layers in solar energy conversion applications. While the ITO/P3HT brush/P3HT-PCBM/Ca/Al solar cell has a lower open circuit voltage, V_{oc}, and fill factor, FF, compared to the typical ITO/PEDOT:PSS/P3HT-PCBM/Ca/Al device architecture, the short-circuit current, J_{sc}, of the P3HT brush device is nearly double that of the control cell, resulting in similar PCEs. One possible explanation for the change produced by the P3HT brush is that the chemical attachment of the P3HT chains to the

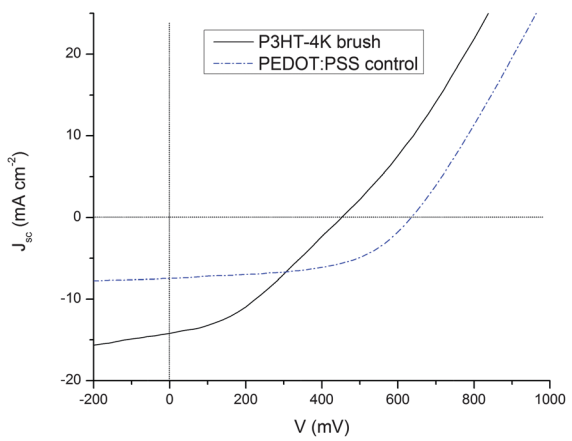

Fig. 6 *I–V* curves measured for the ITO/PEDOT:PSS/P3HT-PCBM/Ca/Al control solar cell (dot–dash curve) and the ITO/P3HT-4K brush/P3HT-PCBM/Ca/Al (solid curve) under AM1.5G illumination. The brush-modified device shows a considerable increase in short circuit current relative to the device made using PEDOT:PSS as an anode buffer layer.

Table 2 Performance characteristics of OPV devices made with PEDOT:PSS and P3HT-4K brush buffer layers

Anode buffer layer	J_{sc} (mA cm^{-2})	V_{oc} (V)	FF	PCE
PEDOT:PSS	7.48	0.64	0.53	2.54
P3HT-4K	14.20	0.46	0.35	2.27

ITO substrate has resulted in depletion of PCBM near the anode, leaving a donor-rich material in contact with the anode. Additionally, the preferential upright orientation of the P3HT chains induced by grafting may increase hole mobility toward the electrode, contributing favorably to charge extraction. A similar effect was reported by Xue *et al.*, who observed that slowing the post-annealing cooling rate of OPV devices based on P3HT–PCBM blends led to small improvements in J_{sc} (changes of ~1–3 mA cm^{-2}).[50] The changes in J_{sc} were correlated with increases in vertical alignment of P3HT chains at the interface between the PEDOT:PSS buffer layer and the BHJ film, which was interpreted from near edge X-ray absorption fine structure (NEXAFS) spectroscopy.

In addition to the importance of interfacial structure on charge transfer, it is understood that changing the chemistry of the anode buffer layer can improve J_{sc}. Examples of this include changing the type of PEDOT:PSS used or adjusting the stoichiometry of the mixture,[11] chemically modifying the PEDOT material,[16] or inserting a P3HT film between the PEDOT:PSS anode buffer layer and the P3HT/PCBM active layer.[17] The increases in J_{sc} seen in these situations are typically accompanied by lower V_{oc} and FF values, suggesting that the anode buffer layer affects charge injection and the internal electric field distribution.[11,16] Of course, these changes may also alter the nanoscale morphology and vertical segregation of the active layer, which can lead to a decrease in device performance.[5,16,17,51] With this in mind, the advantage of the P3HT brush-based anode buffer layers appears to reside in the potential of P3HT brushes to serve as buffer layers that result in a material homojunction yet offer an electronic heterojunction caused by the formation of a surface dipole.[52] A detailed account of how surface electrostatics are affected by the presence of surface monolayers and are dependent on their molecular orientation is offered in a recent review by Heimel *et al.*[53] Particularly germane are recent computational studies showing that the frontier electronic states of P3HT monolayers are impacted by the orientation angle between the chain backbones and the confining surface[54] as well as studies showing that surface dipoles resulting from molecular assemblies of thiophene oligomers lying coincident with or perpendicular to the plane of the surface dramatically impact electronic structure and device-relevant properties.[55] Thus, not only do the P3HT brushes lead to a marked increase in J_{sc} and eliminate the drawbacks of PEDOT:PSS, but from a fundamental point-of-view, these model systems may be useful in teasing apart the complex, intertwined connections between structure and properties of the anode buffer layer, morphology of the active layer, and device performance without altering the chemistry at the electrode-active layer interface.

Conclusions

End-functionalized, regioregular P3HT chains were used to create P3HT brushes on a variety of oxide surfaces. Dense, uniform interfacial layers are formed, and control of layer thickness and grafting density is afforded by manipulating the annealing temperature used during the brush formation process. While confinement and tethering may alter the aggregation state of the chains, as evidenced from optical absorbance measurements, OPV devices created with anode-modifying P3HT brushes, rather than PSS:PEDOT layers, show a remarkable improvement in the short circuit current, which suggests that these interfacial, hole-transporting layers offer considerable potential in solar cell devices. Additional efforts to examine the phase separation of PCBM and P3HT bulk heterojunction thin films coated atop P3HT brush buffer layers and the impact of grafting density, molecular weight and processing conditions on structure–property–performance relationships are underway. These findings and future studies underscore the continued utility of polymer brushes as model systems, even in situations where the polymeric materials are somewhat intractable due to rigidity or limited solubility.

Acknowledgements

WMK and SMKII acknowledge support from a NSF RII grant (NSF EPSCoR EPS 1004083) that enabled the syntheses of the polymers used herein and DL acknowledges support from NSF (award #ECCS-1151140). A portion of this research was sponsored by the Laboratory Directed Research and Development Program of Oak Ridge National Laboratory, managed by UT-Battelle, LLC, for the U. S. Department of Energy. A portion of this research was conducted at the Center for Nanophase Materials Sciences and at the Spallation Neutron Source, which are sponsored at Oak Ridge National Laboratory by the Scientific User Facilities Division, Office of Basic Energy Sciences, U.S. Department of Energy.

Notes and references

1 C. Deibel and V. Dyakonov, *Rep. Prog. Phys.*, 2010, **73**, 096401.
2 A. J. Moule and K. Meerholz, *Adv. Funct. Mater.*, 2009, **19**, 3028–3036.
3 Y. Yao, J. H. Hou, Z. Xu, G. Li and Y. Yang, *Adv. Funct. Mater.*, 2008, **18**, 1783–1789.
4 S. S. van Bavel, M. Barenklau, G. de With, H. Hoppe and J. Loos, *Adv. Funct. Mater.*, 2010, **20**, 1458–1463.
5 D. S. Germack, C. K. Chan, B. H. Hamadani, L. J. Richter, D. A. Fischer, D. J. Gundlach and D. M. DeLongchamp, *Appl. Phys. Lett.*, 2009, **94**, 233303.
6 D. S. Germack, C. K. Chan, R. J. Kline, D. A. Fischer, D. J. Gundlach, M. F. Toney, L. J. Richter and D. M. DeLongchamp, *Macromolecules*, 2010, **43**, 3828–3836.
7 J. W. Kiel, M. E. Mackay, B. J. Kirby, B. B. Maranville and C. F. Majkrzak, *J. Chem. Phys.*, 2010, **133**, 074902.
8 A. J. Parnell, A. D. F. Dunbar, A. J. Pearson, P. A. Staniec, A. J. C. Dennison, H. Hamamatsu, M. W. Skoda, D. G. Lidzey and R. A. L. Jones, *Adv. Mater.*, 2010, **22**, 2444–2447.
9 R. Steim, F. R. Kogler and C. J. Brabec, *J. Mater. Chem.*, 2010, **20**, 2499–2512.
10 R. Po, C. Carbonera, A. Bernardi and N. Camaioni, *Energy Environ. Sci.*, 2010, **4**, 285–310.
11 F. L. Zhang, A. Gadisa, O. Inganas, M. Svensson and M. R. Anderson, *Appl. Phys. Lett.*, 2004, **84**, 3906–3908.
12 P. Mansky, Y. Liu, E. Huang, T. P. Russell and C. J. Hawker, *Science*, 1997, **275**, 1458–1460.
13 M. J. Fasolka and A. M. Mayes, *Annu. Rev. Mater. Res.*, 2001, **31**, 323–355.
14 H. Yan, P. Lee, N. R. Armstrong, A. Graham, G. A. Evmenenko, P. Dutta and T. J. Marks, *J. Am. Chem. Soc.*, 2005, **127**, 3172–3183.
15 Y. Sun, M. Wang, X. Gong, J. H. Seo, B. B. Y. Hsu, F. Wudl and A. J. Heeger, *J. Mater. Chem.*, 2011, **21**, 1365–1367.
16 Y. S. Kim, J. H. Park, S.-H. Lee and Y. Lee, *Sol. Energy Mater. Sol. Cells*, 2009, **93**, 1398–1403.
17 C.-W. Liang, W.-F. Su and L. Wang, *Appl. Phys. Lett.*, 2009, **95**, 133303.
18 S. T. Milner, T. A. Witten and M. E. Cates, *Macromolecules*, 1988, **21**, 2610–2619.
19 F. Zhou and W. T. S. Huck, *Phys. Chem. Chem. Phys.*, 2006, **8**, 3815–3823.
20 B. Zhao and W. J. Brittain, *Prog. Polym. Sci.*, 2000, **25**, 677–710.
21 S. T. Milner, *Science*, 1991, **251**, 905–914.
22 S. M. Kilbey, H. Watanabe and M. Tirrell, *Macromolecules*, 2001, **34**, 5249–5259.
23 J. Alonzo, Z. Y. Huang, M. Liu, J. W. Mays, R. G. Toomey, M. D. Dadmun and S. M. Kilbey, *Macromolecules*, 2006, **39**, 8434–8439.
24 Z. Huang, J. Alonzo, M. Liu, H. Ji, F. Yin, G. D. Smith, J. W. Mays, S. M. Kilbey and M. D. Dadmun, *Macromolecules*, 2008, **41**, 1745–1752.
25 J. Alonzo, J. W. Mays and S. M. Kilbey, *Soft Matter*, 2009, **5**, 1897–1904.
26 P. Paoprasert, J. W. Spalenka, D. L. Peterson, R. E. Ruther, R. J. Hamers, P. G. Evans and P. Gopalan, *J. Mater. Chem.*, 2010, **20**, 2651–2658.
27 N. Doubina, J. L. Jenkins, S. A. Paniagua, K. A. Mazzio, G. A. MacDonald, A. K.-Y. Jen, N. R. Armstrong, S. R. Marder and C. K. Luscombe, *Langmuir*, 2012, **28**, 1900–1908.
28 T. Beryozkina, K. Boyko, N. Khanduyeva, V. Senkovskyy, M. Horecha, U. Oertel, F. Simon, M. Stamm and A. Kiriy, *Angew. Chem., Int. Ed.*, 2009, **48**, 2695–2698.
29 S. K. Sontag, N. Marshall and J. Locklin, *Chem. Commun.*, 2009, 3354–3356.
30 J. Alonzo, J. Chen, J. M. Messman, X. Yu, K. Hong, S. Deng, O. Swader, M. Dadmun, J. F. Ankner, P. Britt, J. W. Mays, M. Malagoli, B. G. Sumpter, J. L. Brédas and S. M. Kilbey, *Chem. Mater.*, 2011, **23**, 4367–4374.
31 J. Liu, R. S. Loewe and R. D. McCullough, *Macromolecules*, 1999, **32**, 5777–5785.
32 M. Jeffries-El, G. Sauve and R. D. McCullough, *Adv. Mater.*, 2004, **16**, 1017–1019.

33 W. M. Kochemba, D. L. Pickel, J. D. Keene, S. J. Rosenthal, B. G. Sumpter, J. H. Chen and S. M. Kilbey, *Chem. Mater.*, 2012, **24**, 4459–4467.
34 W. M. Kochemba, S. M. Kilbey and D. L. Pickel, *J. Polym. Sci., Part A: Polym. Chem.*, 2012, **50**, 2762–2769.
35 J. T. Sullivan, K. E. Harrison, J. P. Mizzell and S. M. Kilbey, *Langmuir*, 2000, **16**, 9797–9803.
36 J. DeWinter, G. Deshayes, F. Boon, O. Coulembier, P. Dubois and P. Gerbaux, *J. Mass Spectrom.*, 2011, **46**, 237–246.
37 R. D. McCullough and R. D. Lowe, *J. Chem. Soc., Chem. Commun.*, 1992, **1**, 70–72.
38 T.-A. Chen, X. Wu and R. D. Rieke, *J. Am. Chem. Soc.*, 1995, **117**, 233–244.
39 G. W. Heffner and D. S. Pearson, *Macromolecules*, 1991, **24**, 6295–6299.
40 The approximate P3HT monomer length was determined from a full geometry optimization of a P3HT oligomer (consisting of 12 monomers) using the MM3 force field, which is described by N. L. Allinger, Y. H. Yuh and J.-H. Lii, *J. Am. Chem. Soc.*, 1989, **111**, 8551–8566.
41 During the course of review of this work, a persistence length of 2.9 nm was reported for regioregular P3HT in *o*-dichlorobenzene: B. McCulloch, V. Ho, M. Hoarfroast, C. Stanley, C. Do, W. T. Heller and R. A. Segalman, *Macromolecules*, 2013, **46**, 1899–1907. This persistence length decreases the calculated $d/2R_g$ and $t/2R_g$ values by only ~6%.
42 K. S. Iyer and I. Luzinov, *Macromolecules*, 2004, **37**, 9538–9545.
43 P. J. Brown, D. S. Thomas, A. Kohler, J. S. Wilson, J. S. Kim, C. M. Ramsdale, H. Sirringhaus and R. H. Friend, *Phys. Rev. B: Condens. Matter Mater. Phys.*, 2003, **67**, 064203.
44 F. Spano, *J. Chem. Phys.*, 2005, **122**, 234701.
45 D. M. DeLongchamp, R. J. Kline, D. A. Fischer, L. J. Richter and M. F. Toney, *Adv. Mater.*, 2011, **23**, 319–337.
46 R. Rajendran, T. Tscuhiya, S. Hirata and T. D. Iordanov, *J. Phys. Chem. A*, 2012, **116**, 12153–12162.
47 M. C. Zerner, in *Reviews in Computational Chemistry*, ed. K. B. Lipkowitz and D. B. Boyd, VCH, New York, 2007, vol. II, p. 313.
48 G. M. Pearl, M. C. Zerner, A. Broo and J. McKelvey, *J. Comput. Chem.*, 1998, **19**, 781–796.
49 B. Sumpter, P. Kumar, A. Mehta, M. D. Barnes, W. Shelton and R. J. Harrison, *J. Phys. Chem. B*, 2005, **109**, 7671–7685.
50 B. F. Xue, B. Vaughan, C. H. Poh, K. B. Burke, L. Thomsen, A. Stapleton, X. J. Zhou, G. W. Bryant, W. Belcher and P. C. Dastoor, *J. Phys. Chem. C*, 2010, **114**, 15797–15805.
51 S. K. Hau, H.-L. Yip, O. Acton, N. S. Baek, H. Ma and A. K.-Y. Jen, *J. Mater. Chem.*, 2008, **18**, 5113–5119.
52 A. Tada, Y. Geng, Q. Wei, K. Hashimoto and K. Tajima, *Nat. Mater.*, 2011, **10**, 450–455.
53 G. Heimel, I. Salzmann, S. Duhm and N. Koch, *Chem. Mater.*, 2011, **23**, 359–377.
54 G. Heimel, I. Salzmann, S. Duhm, J. P. Rabe and N. Koch, *Adv. Funct. Mater.*, 2009, **19**, 3874–3879.
55 S. Duhm, G. Heimel, I. Salzmann, H. Glowatzki, R. L. Johnson, A. J. Vollmer, J. P. Rabe and N. Koch, *Nat. Mater.*, 2008, **7**, 326–332.

